Effect of a Shallow Water Obstruction on Long Wave Runup and Overland Flow Velocity

Patrick J. Lynett[1]

Abstract: A study is presented to examine the one-horizontal dimension effect of a shallow shelf obstacle on nonlinear long wave runup. Due to the large horizontal-vertical aspect ratio of this problem, it is not well suited for experimental analysis, and therefore this study is purely numerical. Simulations are performed for various incident wave conditions, obstacle height and widths, and final beach slopes. Many of the setups involve breaking, either through approaching the obstacle as a large breaking bore, incipient breaking on top of the obstacle, or breaking during the beach uprush. The general conclusion of this study is that, for highly nonlinear waves (ϵ=wave height/shelf water depth $\geq$0.5), the obstacle will always act to reduce the runup and the maximum overland velocity. However, for very small obstacle lengths, particularly for extremely large waves, this reduction may be practically inconsequential. Interestingly, for weakly nonlinear waves ($\epsilon \approx 0.1$), due to front steepening over the obstacle, greater overland velocities can result from increasing obstacle length. Consistent with previous studies, it is found that the final beach slope is of primary importance for determining the runup.

DOI: 10.1061/(ASCE)0733-950X(2007)133:6(455)

CE Database subject headings: Tsunamis; Wave runup; Reefs; Numerical models; Velocity; Overland flow.

Introduction

As a nonlinear long wave, such as a tsunami, approaches the shoreline, it inevitably interacts with any coastal features in its path, such as reefs, bars, and dunes. The role of these obstacles, as noted in a handful of post-tsunami surveys, appears to be as an energy reducer: areas protected by these obstacles tended to experience lower runup and flow velocities. However, most of these field observations are, by nature, qualitative and limited.

Synolakis et al. (1995), surveying the coast of Nicaragua for information about the 1992 tsunami in the region, noted that the highest levels of damage along a particular stretch of beach were located directly landward of a reef opening used for boat traffic. It was postulated that the reef gap acted as a lower resistance conduit for tsunami energy, behaving like a funnel and focusing the tsunami wave. Along neighboring beaches with intact reefs, the tsunami did not have the intensity to remove even beach umbrellas. Investigating impacts from the same tsunami, Borrero et al. (1997), discussed how small scale bathymetry variations affected coastal inundation. One of the conclusions of this work was that bathymetry features with lengthscales 50 m and less had leading order impact on the runup. Looking to the recent Indian Ocean tsunami, a survey team in Sri Lanka inferred from observations that reef and dune breaks lead to locally increased tsunami impact (Liu et al. 2005). Also in Sri Lanka, Fernando et al. (2005) performed a more thorough survey along the southeastern coastline, and concluded that there was a compelling correlation between coral mining and locally severe tsunami damage.

Analytical, experimental, and numerical investigations into the effect of a shallow water obstacle on nonlinear long wave evolution are sparse. Analytical methods, such as Kanoglu and Synolakis (1998), have found that small-scale bathymetry changes do impact the runup. Additionally, these authors note that runup is largely controlled by the last slope a long wave experiences, the beach slope. Such analytical methods are often limited to linear or very long waves, and examination of breaking waves are generally restricted to experimental or numerical studies. Experimental and numerical studies of wave interaction with coastal obstacles (e.g., overtopping) exist in the literature (e.g., Hu et al. 2000), however these focus on wind waves having wavelengths and periods one or more orders of magnitude less than that of a typical tsunami.

When modeling tsunami runup and inundation, a solitary wave is placed in the deep water of the physical or numerical wave tank (e.g., Liu et al. 1995; Li and Raichlen 2002). The initial hurdle to overcome is the vertical-to-horizontal aspect ratio of the long wave problem. A large tsunami may be hundreds of water depths in length—a difficult setup to recreate in the lab. To show the difficulty in studying the impact of a shallow water obstacle in these setups, consider that the model deep water, say 1 m, is meant to represent the oceanic deep water, on the order of 1,000 m. To experimentally assess the impact of a full-scale obstacle that is 100 m long, 10 m high, in a water depth of 10 m, the model obstacle would be just 10 cm long, 1 cm high, in 1 cm water depth, and scale effects would render the results difficult to interpret. To make the situation even more difficult, the most relevant problem occurs when the obstacle height is in the same order as the wave height.

It is the purpose of this paper to examine this physical problem through numerical means, where performing simulations with huge aspect ratios are computationally possible. The focus here will be on how shallow water obstacles affect the runup and overland flow velocities of nonlinear long waves. In the following

[1]Assistant Professor, Dept. of Civil Engineering, Texas A&M Univ., College Station, TX 77843-3136. E-mail: plynett@tamu.edu

Note. Discussion open until April 1, 2008. Separate discussions must be submitted for individual papers. To extend the closing date by one month, a written request must be filed with the ASCE Managing Editor. The manuscript for this paper was submitted for review and possible publication on August 25, 2005; approved on November 6, 2006. This paper is part of the ***Journal of Waterway, Port, Coastal, and Ocean Engineering***, Vol. 133, No. 6, November 1, 2007. ©ASCE, ISSN 0733-950X/2007/6-455–462/$25.00.

section, the numerical basis will be presented. Next, the results of nearly 1,000 simulations will be discussed, for various incident wave conditions, obstacle height and widths, and final beach slopes.

Numerical Experiment Setup

As mentioned in the "Introduction," the scale of the problem to be investigated here is poorly suited to be studied in a physical wave tank. The horizontal length scale of the wave will be many hundreds of water depths, typical of a tsunami for example, and would be difficult to create in a laboratory without significant scaling issues. Here, a numerical model based on the Boussinesq-type equations will be employed to study long wave evolution over a rough obstacle in shallow water. These equations are derived from a depth integration of the Reynolds averaged Navier–Stokes equations, commonly with the assumption of zero vorticity. The resulting equation model consists of a mass conservation equation and a vector equation for the horizontal velocity components

$$\frac{\partial \zeta}{\partial t} + \nabla \cdot [(\zeta + h)\boldsymbol{u}] - \nabla \cdot \left\{ \left[\frac{\zeta^3 + h^3}{6} - \frac{(\zeta + h)\kappa^2}{2} \right] \nabla S + \left[\frac{\zeta^2 - h^2}{2} - (\zeta + h)\kappa \right] \nabla T \right\} = 0 \tag{1}$$

$$\frac{\partial \boldsymbol{u}}{\partial t} + \frac{1}{2} \nabla (\boldsymbol{u} \cdot \boldsymbol{u}) + g \nabla \zeta + \frac{\partial}{\partial t} \left\{ \frac{\kappa^2}{2} \nabla S + \kappa \nabla T - \nabla \left(\frac{\zeta^2}{2} S \right) - \nabla (\zeta T) \right\} + \nabla \left\{ \frac{\partial \zeta}{\partial t} (T + \zeta S) + (\kappa - \zeta)(\boldsymbol{u} \cdot \nabla) T + \frac{1}{2} (\kappa^2 - \zeta^2)(\boldsymbol{u} \cdot \nabla) S + \frac{1}{2} [(T + \zeta S)^2] \right\} - \boldsymbol{R}_b + \boldsymbol{R}_f + \boldsymbol{R}_{sg} = 0 \tag{2}$$

where

$$S = \nabla \cdot \boldsymbol{u}, \quad T = \nabla \cdot (h\boldsymbol{u}) \tag{3}$$

ζ=free surface elevation; $\boldsymbol{u}$=horizontal velocity vector evaluated at κ and $\kappa = -0.531h$; h=local water depth; g=gravity, $\boldsymbol{R}_b$=breaking-related dissipation term; $\boldsymbol{R}_f$ accounts for bottom friction; and $\boldsymbol{R}_{sg}$ for eddy viscosity dissipation.

As can be seen in Eq. (2), there are three sources of dissipation: bottom friction, breaking, and viscous diffusion. Bottom friction is calculated with the quadratic friction equation

$$\boldsymbol{R}_f = \frac{f}{h + \zeta} \boldsymbol{u}_b |\boldsymbol{u}_b| \tag{4}$$

where $\boldsymbol{u}_b$=velocity evaluated at the seafloor; and f=bottom friction coefficient, typically in the range of 10^{-3}–10^{-2}. To simulate the effects of wave breaking, the eddy viscosity model of Kennedy et al. (2000) is used here with some modification, as given in Lynett (2006). The eddy viscosity formulation, $\boldsymbol{R}_{sg}$, also follows that given in Lynett (2006).

The use of the Boussinesq is chosen over the nonlinear shallow water (NLSW) model based on established equation accuracy (e.g., Madsen and Schaffer 1998). The fundamental supposition is that given identical numerical schemes and setups with convergent numerical results, there is no reason to expect the Boussinesq to be less accurate than the NLSW. This statement permits the possibility that both models are equally (in)accurate and (un)acceptable for a given problem, and neglects the practical consideration that the Boussinesq model requires significantly more computational time to complete a simulation. To test the differences of the two models, four sets of simulations with varying incident wave heights were run with the NLSW, corresponding to the Boussinesq results to be presented later in this paper. The conclusion of this sensitivity study is that for long waves that do not break, differences between NLSW and Boussinesq are negligible. For breaking waves, maximum differences in predicted runup are near 10%. These changes are driven by slightly different interaction between the steep wave front and the breaking model, depending on whether dispersive terms are included. The breaking model employed here is calibrated only with the Boussinesq model (e.g., Lynett 2006), and thus the use of the Boussinesq with this particular breaking model is preferred.

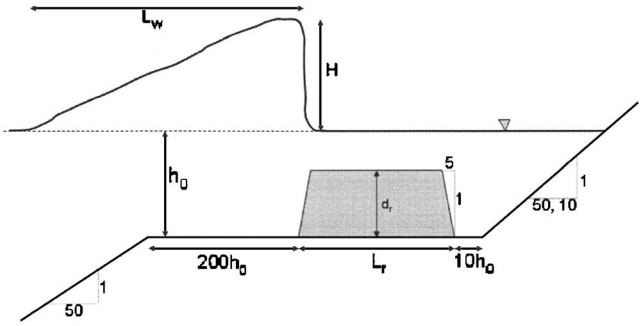

Fig. 1. Problem setup and variable definition

The finite difference algorithm presented in Lynett and Liu (2002) is used to solve the model equations; the scheme is briefly described here. A high-order predictor-corrector scheme is utilized, employing a third order in time explicit Adams–Bashforth predictor step, and a fourth order in time implicit Adams–Moulton corrector step (Press et al. 1992). Spatial derivatives are differenced to fourth-order accuracy, yielding a model which is numerically accurate to $(\Delta x)^4$, $(\Delta y)^4$ in space, and $(\Delta t)^4$ in time.

Accurate prediction of runup and rundown of the waves is of utmost importance to this study. The moving boundary scheme employed here is the technique developed by Lynett et al. (2002). Founded around the restrictions of the high-order numerical wave propagation model, the moving boundary scheme utilizes linear extrapolation of free surface and velocity through the shoreline, into the dry region. This approach allows for the five-point finite difference formulas to be applied at all points, even those neighboring dry points, and thus eliminates the need for conditional statements.

To simulate a realistic shallow water wave condition, a solitary wave is placed in the deeper water portion of the domain. Note that although the solitary wave is placed in the deep water portion of the domain, its form is based on the local depth, and thus is still a long wave initially. The depth in this deep portion is given in the Appendix . The solitary wave then travels up a slope onto a flat shelf with depth h_0, where an obstacle is situated (Fig. 1). After the obstacle, the depth returns to h_0 for a length of $10h_0$. The final transition is the beach slope; two beach slopes, m, will be tested here, a mild $m=1/50$ slope and a steep $m=1/10$. Four different wave conditions will be tested with varying levels of nonlinearity. As the wave height is changing throughout its evolution, the characteristic height H will be that measured at the toe of the obstacle. The four wave conditions have shelf nonlinearity

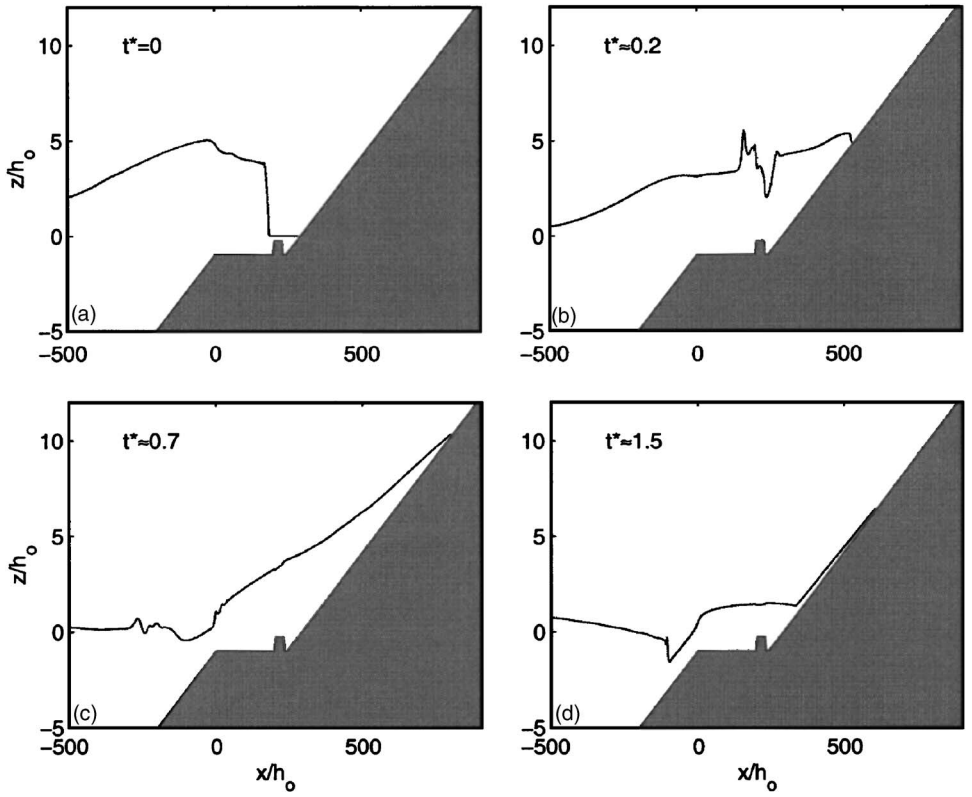

Fig. 2. Spatial snapshots at four different times for extremely nonlinear wave ($\epsilon \approx 4$) propagating over obstacle with $d_r/h_0=0.75$ and $L_r/L_w \approx 0.03$ and running up beach slope $m=1/50$. Dimensionless time, t^*, is defined as $t\sqrt{g(H+h_0)}/L_w$.

$\epsilon=H/h_0$ approximately equal to 0.1, 0.5, 1, and 4.

The obstacle will have the shape of a trapezoid, with side slopes of 1/5. The length of the obstacle L_r, as shown in Fig. 1, will be varied. This length will always be given as a fraction of the incoming wavelength, L_w, measured as given in Fig. 1. It is noted that for the problems to be examined here, the wavelength is not always a clearly defined parameter. The nonlinear long waves develop a very steep front on the shelf, such that the front moves faster than the tail, and the length can change in time. Also due to the long nature of the wave, the entire wave does not exist in the same depth at any particular time. Having this information in mind, wavelength is measured as shown in Fig. 1, taken as the length of the wave when the wave front reaches the obstacle, and should be interpreted as an approximate value.

The height of the obstacle, d_r will also be varied, and will be expressed as a fraction of the shelf depth, i.e., d_r/h_0. To approximate roughness, the obstacle will have a large bottom friction coefficient. The obstacle is given a friction coefficient of 0.01, taken from field studies of wave dissipation over a barrier reef (Lowe et al. 2005). Obstacles of all heights use this friction coefficient. All other locations use a coefficient of 0.002, a reasonable value for a smooth sandy bottom. In a practical sense, this obstacle is meant to approximate a number of coastal structures: a rubble mound for L_r/L_w values near zero, a reef for small to moderate values of L_r/L_w, and possibly an offshore or barrier island for moderate to large L_r/L_w. It is noted here that this study is only investigating the one horizontal dimension (1HD) effect of an obstacle. The two horizontal dimension (2HD) impact, due to, for example, a break in a reef is not examined here, but may be significant.

A simulation example is given in Fig. 2. In this figure, snapshots for an extremely nonlinear wave ($\epsilon=H/h_0 \approx 4$) evolving over a relatively short obstacle ($L_r/L_w \approx 0.03$) are shown. As seen in Fig. 2(a), the incoming wave has broken before the shelf break, and is a fully developed bore before reaching the obstacle. The bore hits the obstacle, and a small amount of this leading energy is reflected offshore [Fig. 2(b)]. As the wave rushes onshore, the front remains as a steep breaking bore until maximum runup is reached, shown in Fig. 2(c). Rundown is characterized by a relatively thin layer of fluid [Fig. 2(d)], but with very high velocity. The magnitude of this rundown velocity will be strongly dependent on the bottom roughness and the slope of the beach.

The analysis in the following section will focus on two particular aspects of this complex flow problem: maximum runup, R, and maximum overland velocity, $U_{\max}$. Maximum runup is a vertical distance and clearly defined. Runup will be scaled by the shelf wave height, H. Maximum overland velocity is the maximum horizontal uprush velocity experienced on initially dry land. Generally, this maximum velocity is located very near to the initial shoreline position, and occurs as the leading wave front begins running up the slope. Velocity will be scaled by the shelf linear long wave speed, $c_0=\sqrt{gh_0}$.

Results and Discussion

In this section, the impact of a rough obstacle on nonlinear long wave runup and overland velocity will be quantitatively assessed. Four different incident wave conditions will be examined, propagating over a wide range of obstacle height and width. For these simulations, the numerical grid spacing, Δx, lies in the range of

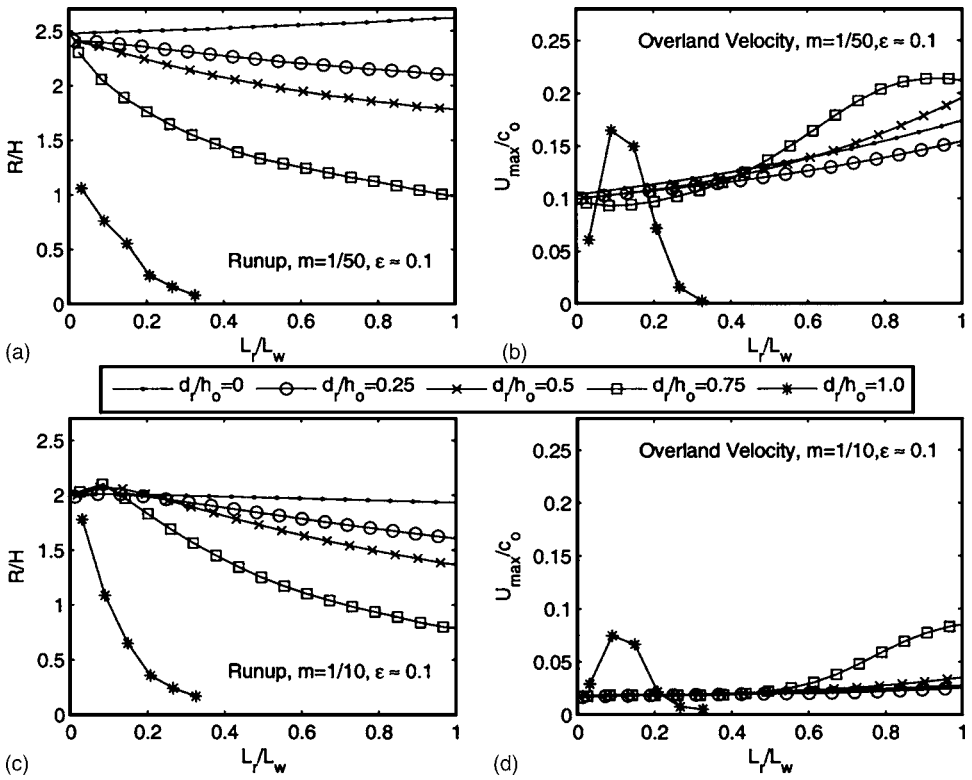

Fig. 3. Scaled runup and maximum overland velocity for incident wave with $\epsilon \approx 0.1$ and $L_w/h_0 \approx 500$ for variable obstacle height and length. Curves with dots are for $d_r/h_0=0$, circles are for $d_r/h_0=0.25$, crosses are for $d_r/h_0=0.5$, squares are for $d_r/h_0=0.75$, and stars are for $d_r/h_0=1.0$.

$0.5-1.5h_0$, and select simulations (those with the smallest L_r and highest d_r for each wave condition) have been tested for numerical convergence. The first wave condition to be discussed will be the condition with the weakest nonlinearity.

Weakly Nonlinear Incident Wave, $\epsilon = H/h_0 \approx 0.1$

Fig. 3 shows how runup and uprush velocity vary with obstacle length and height. A curve is given for four obstacle heights from $d_r/h_0=0.25$ to 1. An additional curve is given for $d_r/h_0=0$, which is the case for no obstacle and constant bottom friction coefficient of 0.002 everywhere in the domain. This curve is meant to represent the "baseline" runup and velocity, to which the others can be compared to quantify the impact of the obstacle. For example, looking to subplots (a) and (b) for beach slope 1/50, and obstacle with height $d_r/h_0=0.75$ and length $L_r/L_w=0.8$, the obstacle reduces runup by about 55% and increases velocity by 30% as compared to the same setup with the obstacle removed.

There are a number of unique patterns for this case that will not be as apparent for waves with higher nonlinearity. For the mild slope case ($m=1/50$), the runup and velocity for the baseline setup increase as the shelf length increases. While it might be reasonably expected that runup and velocity decrease with increasing shelf length, due to increased bottom friction dissipation, here this is not always the case. Note that, for example, with $L_r/L_w \approx 1$ and the specified $L_w/h_0 \approx 500$, the total shelf length is approximately $710h_0$. With the combined shelf and mild slope, amplitude dispersion has enough time, even for the weakly nonlinear wave, to steepen the wave front, leading to increased runup and overland velocities. Comparing this to the steep slope ($m=1/10$) baseline case where this trend does not exist, it is evident that the milder slope is driving most of the steepening, rather than the shelf. In fact, looking to the steep slope baseline case, the runup results show that the wave feels the slope in much the same way as it would a vertical wall, such that runup is twice the wave height. Likewise, the maximum velocities for the steep slope cases are very low. Clearly the final beach slope is of primary importance when predicting runup and velocity.

For this weakly nonlinear wave, the reverse trends in runup and velocity (one decreases while the other increases) are also explained by wave front steepening. The obstacles lead to decreased runup and increased velocity up to some threshold obstacle length. The threshold length for the obstacle with $d_r/h_0=1$ is $L_r/L_w \approx 0.12$ and for $d_r/h_0=0.75$ the threshold is $L_r/L_w \approx 0.95$. This phenomenon is explained in Fig. 4, showing waveforms for a setup with and without an obstacle. In Fig. 4(a), without the obstacle, the solitary wave changes slightly over the shelf as amplitude dispersion mildly steepens the front and bottom friction reduces the amplitude. With the obstacle, in Fig. 4(b), some of the incident energy is reflected out to sea by the offshore side of the obstacle. Additionally, the much shallower depth increases the importance of bottom friction, and the wave height is much reduced before reaching the beach. Also, however, due to the shallower depth, nonlinearity is more important, and front steepening is more significant. This front does not break, but does form a weak undular bore type structure. When this steeper front reaches the beach, the result is higher flow velocities, but much decreased runup. There are clear engineering implications here: for this weakly nonlinear wave, it is in fact possible for an obstacle, such as a reef, to increase the magnitude of overland

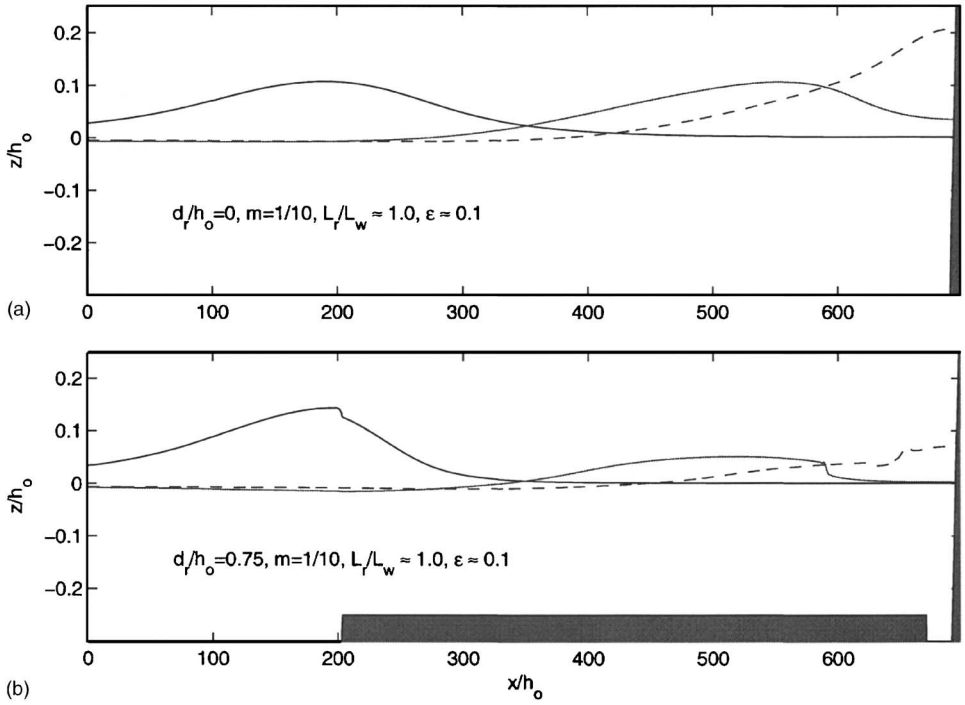

Fig. 4. Comparisons of wave forms for two different setups, one without obstacle (a); one with obstacle (b). Snapshots at three different times are shown, first with crest at $x/h_0=200$, second with crest near $x/h_0=600$, and last (dashed line) at time of maximum runup. Top of obstacle can be seen in (b) as gray area between $x/h_0=200$ and 680.

velocities (and related transport) while decreasing inundation limits. This will not be the case for waves with higher incident nonlinearity.

Highly Nonlinear Incident Waves, $\epsilon=H/h_0\approx 0.5$ and $\epsilon=H/h_0\approx 1$

These two wave conditions are grouped together as they behave in a very similar manner. Figs. 5 and 6 give the results for these two wave conditions. For the mild slope cases, there is a very regular pattern of decreased runup with increased obstacle length and height. Velocity does not behave as monotonically. There appears to be an "optimum" obstacle length that results in maximum velocities, which decreases with increasing obstacle height. For example, with an obstacle height of $d_r/h_0=0.5$, the maximum overland velocity occurs when $L_r/L_w\approx 0.15$. This maximum occurs due to the wave height over the shelf, controlled by reflection off the seaward obstacle face and bottom friction, and depth above the obstacle, which when combined govern the strength of amplitude dispersion and steepening. Note that, for all cases, the runup and overland velocity is less than that for the baseline, showing that for these highly nonlinear waves, an obstacle appears to always lead to a reduction in tsunami impact on the beach.

For the steep slope cases, the trends show different behavior for small obstacle length as compared to the mild slope. Runup and overland velocity show weak dependency on obstacle height for $L_r/L_w<0.1$, as shown by the converging trends. The interesting cause of this behavior is a resonance that occurs in between the beach and the reef. This process is shown in Fig. 7. Wave energy reflected off the beach is re-reflected off the landward side of the obstacle, combining with the incident wave propagating landward. In the figure there are two distinct runup maxima in (c) and (e), where the first maxima is due to the runup of the wave front and the second, and larger, maxima is due to this re-reflection effect. The efficiency of this re-reflection is related to d_r, while the amount of energy passing over the obstacle is inversely related to d_r. These two factors work against each other to create a large runup at small L_r/L_w, regardless of obstacle height. The effect is most significant when the wave height, water depth, and obstacle height are all similar values. This resonance is inhibited by a milder slope, and does not play a significant role in the $m=1/50$ cases.

Extremely Nonlinear Incident Wave, $\epsilon=H/h_0\approx 4$

Finally, the interaction between a rough obstacle and a very large incident wave is examined. An example of this condition has been given in Fig. 2. Note that the wavelength of this wave is twice as large as the three previous wave conditions. The reason for this is that it was not possible to maintain the extremely high nonlinearity without also increasing the wavelength. The runup and uprush velocity trends are shown in Fig. 8. The behavior shown in this figure is the most regular of all the cases given, with runup and velocity decreasing steadily with increasing obstacle length and height.

There are a couple of interesting results from this analysis. One is that for very small obstacle lengths, $L_r/L_w<0.02$, the effect of the obstacle diminishes; runup and velocity approach the baseline values. The explanation for this is that the wave height is so much larger than the obstacle height, and thus the offshore directed reflection is relatively small. Also note that the runup and velocity trends shown in Fig. 8 for nonzero obstacle heights lie closer together as compared to other wave nonlinearities. It follows then that the amount of energy reaching the beach for extremely nonlinear waves will be primarily controlled not by wave reflections off bathymetry features but dissipation mechanisms, namely bore front breaking and bottom friction.

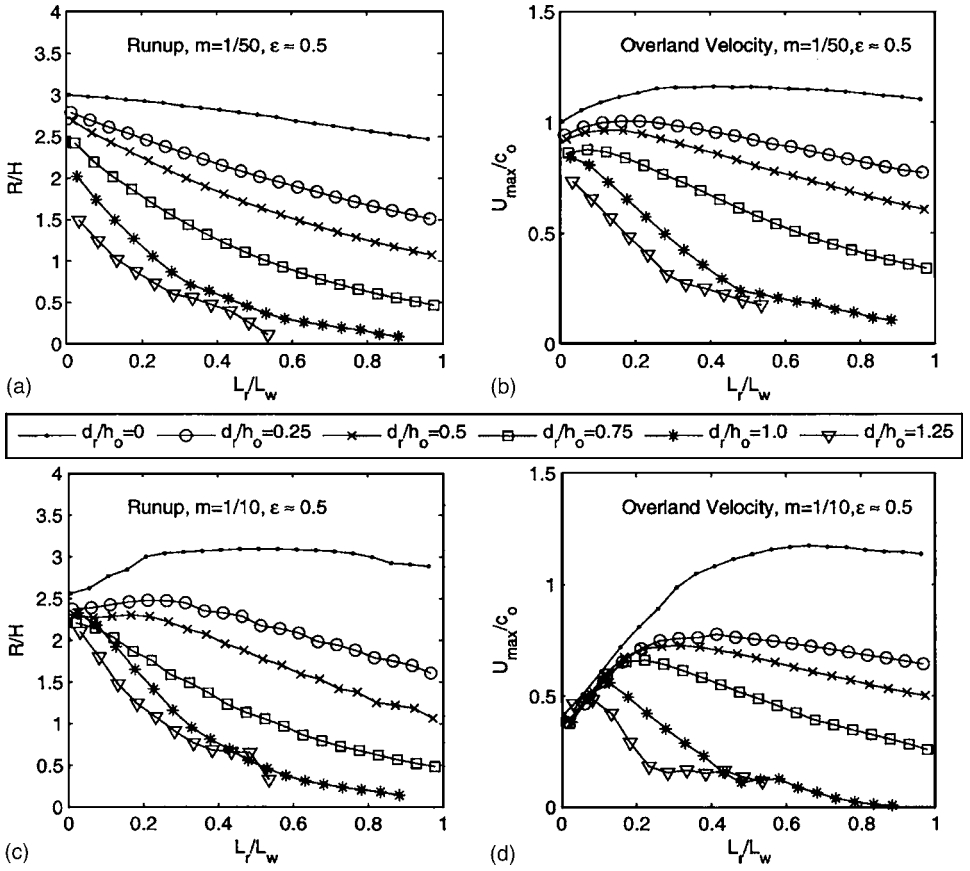

Fig. 5. Scaled runup and maximum overland velocity for incident wave with $\epsilon \approx 0.5$ and $L_w/h_0 \approx 500$ for variable obstacle height and length. Curves as for Fig. 3 with triangles for $d_r/h_0 = 1.25$.

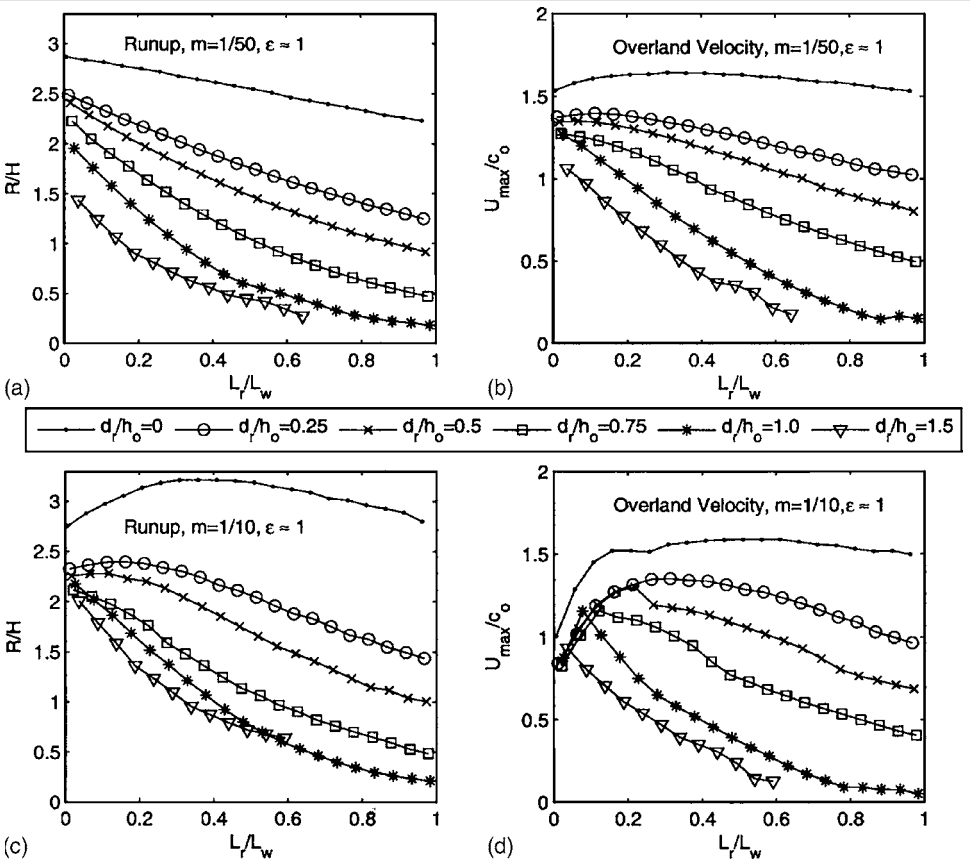

Fig. 6. Scaled runup and maximum overland velocity for incident wave with $\epsilon \approx 1$ and $L_w/h_0 \approx 500$ for variable obstacle height and length. Curves as for Fig. 3 with triangles for $d_r/h_0 = 1.5$.

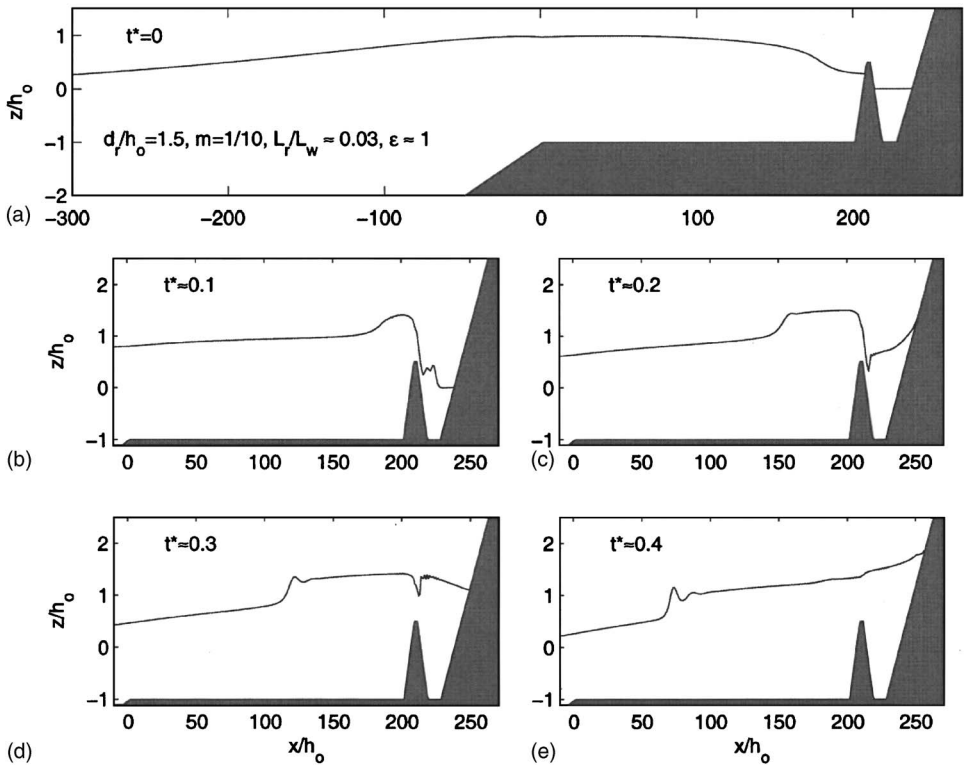

Fig. 7. Spatial snapshots at five different times for highly nonlinear wave ($\epsilon \approx 1$) propagating over obstacle with $d_r/h_0 = 1.5$ and $L_r/L_w \approx 0.03$ and running up beach slope $m = 1/10$. Note two runup maxima in (c) and (e), with (e) showing later and larger of two. Dimensionless time, t^*, is defined as $t\sqrt{g(H+h_0)}/L_w$.

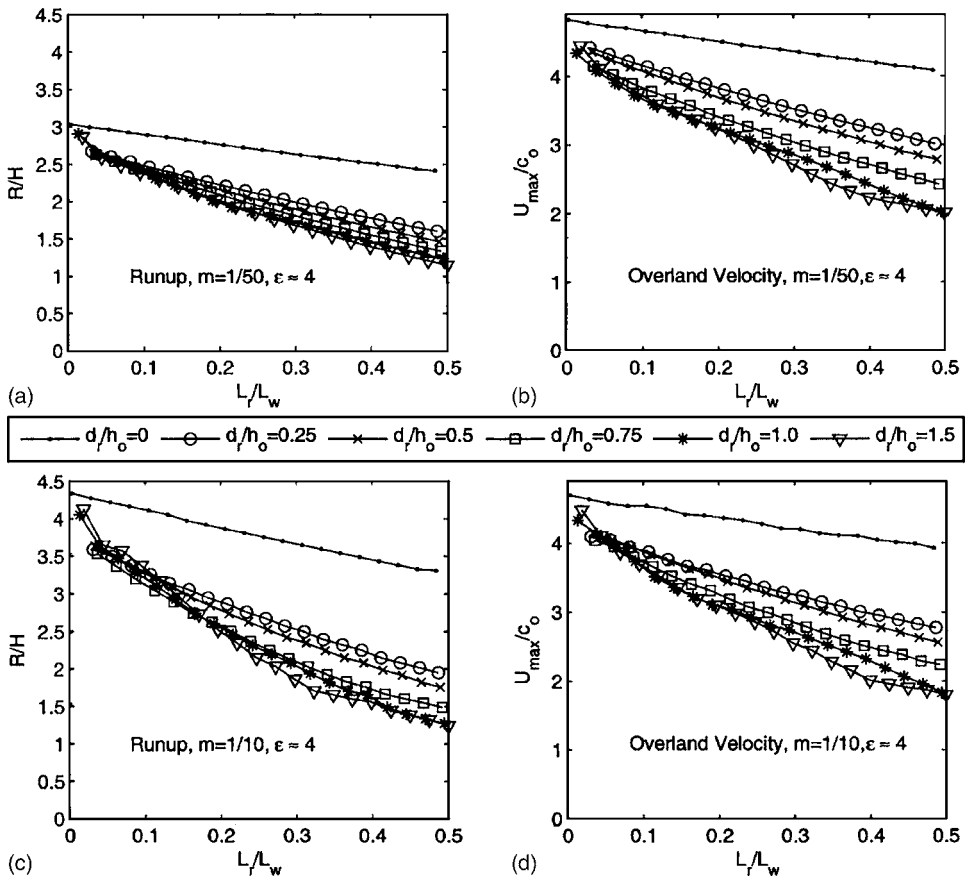

Fig. 8. Scaled runup and maximum overland velocity for incident wave with $\epsilon \approx 4$ and $L_w/h_0 \approx 1{,}000$ for variable obstacle height and length. Curves as for Fig. 3 with triangles for $d_r/h_0 = 1.5$.

Table 1. Numerical Simulation Parameters

Shelf nonlinearity	h/h_0	H_{dw}/h	$\Delta x/h_0$
$\epsilon=H/h_0\approx 0.1$	20	0.0035	0.5
$\epsilon=H/h_0\approx 0.5$	45	0.007	1.0
$\epsilon=H/h_0\approx 1$	60	0.01	1.0
$\epsilon=H/h_0\approx 4$	100	0.045	1.5

The importance of the final beach slope is again underscored here. Recall from the weakly nonlinear condition that showed runup on a steep slope was less than that on a mild slope, due to the decreased time possible for steepening. Here, for the extremely nonlinear case, the reverse is evident. Runup on the steep slope is larger, reaching values of over four times the shelf wave height for a short shelf. The steeper, and shorter slope provides less time for the bore front and bottom friction to dissipate energy during runup. More of the incoming kinetic energy can be converted into potential, and the runup is greater.

Conclusions

A numerical study, comprising 920 simulations, was undertaken to examine the effect of a shelf obstacle on nonlinear long wave runup. Tsunami waves with four shelf nonlinearities, ranging from 0.1 to 4, were examined over a wide range of obstacle heights, obstacle lengths, and final beach slopes. Many of the setups involve breaking, either through approaching the obstacle as a large breaking bore, incipient breaking on top of the obstacle, or breaking during the beach uprush. A Boussinesq wave model with a calibrated and established breaking model is employed for the numerical simulations. The general conclusion of this study is that, for highly nonlinear waves ($\epsilon \geq 0.5$), the obstacle will always act to reduce the runup and the maximum overland velocity. However, for very small obstacle lengths, particularly for extremely large waves, this reduction may be practically inconsequential. Interestingly, for weakly nonlinear waves ($\epsilon \approx 0.1$), due to front steepening over the obstacle, greater overland velocities can result with long obstacle lengths. Again, though, even for weakly nonlinear waves, reduced runup should be expected. Consistent with previous studies, it is found that the final beach slope is of primary importance for determining the runup. For weakly nonlinear, nonbreaking tsunami waves, the largest runup occurred on the mildest beach slope. Inversely, for the extremely nonlinear, strongly breaking waves, the largest runup was found on the steepest beach slope.

The work here focuses on 1HD effects, and thus would be applicable to, for example, nearshore regions characterized by long and continuous reefs or breakwaters. 2HD effects due to alongshore breaks in such systems need to be quantified in a similar manner as done here or through site-specific numerical modeling. These breaks, as observed in tsunami field studies (e.g. Liu et al. 2005), despite widths of a small fraction of the wavelength, can lead to significantly increased runup and flow velocities. Local 2HD features, such as these, should be considered when applying the data contained in this paper.

Acknowledgments

The research presented here was partially supported by grants from the National Science Foundation (Grant Nos. CBET-0427014 and CMMI-0619083).

Appendix. Numerical Simulation Parameters

Table 1 provides the scaled water depth in the deeper water portion of the domain, h, where the solitary wave is initially located (h/h_0), the scaled wave height of the initial condition, when the solitary wave is depth h (H_{dw}/h), and constant grid length (Δx) for all results presented in this paper. Note that the values given in the table were chosen such that the target nearshore wave height and wavelength resulted.

References

Borrero, J. C., Bourgeois, J., Harkins, G., and Synolakis, C. E. (1997). "How small-scale bathymetry affected coastal inundation in the 1992 Nicaraguan tsunami." *Proc., Fall AGU Meeting*, San Francisco.

Fernando, H. J. S., McCulley, J. L., Mendis, S. G., and Perera, K. (2005). "Coral poaching worsens tsunami destruction in Sri Lanka." *EOS Trans. Am. Geophys. Union*, 86(33), 301.

Hu, K., Mingham, C. G., and Causon, D. M. (2000). "Numerical simulation of wave overtopping of coastal structures using the nonlinear shallow water equations." *Coastal Eng.*, 41, 433–465.

Kanoglu, U., and Synolakis, C. E. (1998). "Long wave runup on piecewise linear topographies." *J. Fluid Mech.*, 374, 1–28.

Kennedy, A. B., Chen, Q., Kirby, J. T., and Dalrymple, R. A. (2000). "Boussinesq modeling of wave transformation, breaking and runup. I: 1D." *J. Waterway, Port, Coastal, Ocean Eng.*, 126(1), 39–47.

Li, Y., and Raichlen, F. (2002). "Nonbreaking and breaking solitary wave runup." *J. Fluid Mech.*, 456, 295–318.

Liu, P. L.-F., et al. (2005). "Observations by the International Tsunami Survey Team in Sri Lanka." *Science*, 308, 1595.

Liu, P. L.-F., Cho, Y. S., Briggs, M. J., Synolakis, C. E., and Kanoglu, U. (1995). "Runup of solitary waves on a circular island." *J. Fluid Mech.*, 302, 259–285.

Lowe, R. J., Falter, J. L., Bandet, M. D., Pawlak, G., Atkinson, M. J., Monismith, S. G., and Koseff, J. R. (2005). "Spectral wave dissipation over a barrier reef." *J. Geophys. Res.*, 110(C4), C04001.

Lynett, P. (2006). "Nearshore modeling with high-order Boussinesq equations." *J. Waterway, Port, Coastal, Ocean Eng.*, 132(5), 348–357.

Lynett, P., and Liu, P. L.-F. (2002). "A numerical study of submarine landslide generated waves and runup." *Proc. R. Soc. London, Ser. A*, 458, 2885–2910.

Lynett, P., Wu, T.-R., and Liu, P. L.-F. (2002). "Modeling wave runup with depth-integrated equations." *Coastal Eng.*, 46(2), 89–107.

Madsen, P. A., and Schaffer, H. A. (1998). "Higher order Boussinesq-type equations for surface gravity waves: Derivation and analysis." *Philos. Trans. R. Soc. London*, 356, 3123–3181.

Press, H. W., Teukolsky, S. A., Vetterling, W. T., and Flannery, B. P. (1992). *Numerical recipes in fortran 77*, 2nd Ed., Cambridge University Press, Cambridge, U.K.

Synolakis, C. E., Imamura, F., Tsuji, Y., Matsutomi, S., Tinti, B., Cook, B., and Ushman, M. (1995). "Damage, conditions of East Java tsunami of 1994 analyzed." *EOS Trans. Am. Geophys. Union*, 76(26), 257, 261–262.